International Journal of Safety and Security Engineering
Vol. 16, No. 10, October, 2026, pp. 2363-2371
Journal homepage: http://iieta.org/journals/ijsse

# An Investigation of Pore-Water Pressure Response and Factor of Safety Degradation in Rainfall-Affected Slopes of Northern Sarawak

Azira Abu Abdul Taip, Raudhah Ahmadi*, Imtiyaz Akbar Najar, Dayang Siti Afiqah Abang Kamarud-din, Rosmina Ahmad Bustami, Dayangku Salma Awang Ismail

Department of Civil Engineering, Faculty of Engineering, University of Malaysia Sarawak, Kota Samarahan 94300, Malaysia

Corresponding Author Email: araudhah@unimas.my

Copyright: ©2026 The authors. This article is published by IIETA and is licensed under the CC BY 4.0 license (http://creativecommons.org/licenses/by/4.0/).

https://doi.org/10.18280/ijsse.161014

**Received:** 24 August 2026
**Revised:** 3 October 2026
**Accepted:** 10 October 2026
**Available online:** 31 October 2026

***Keywords:***
*rainfall infiltration, slope stability, pore-water pressure, Factor of Safety, residual soil, Setap Shale Formation*

**ABSTRACT**

This study investigates the effect of rainfall infiltration on pore-water pressure (PWP) response and slope stability degradation in a residual soil slope situated within the *Setap* Shale Formation of northern Sarawak. Coupled seepage and slope stability analyses were conducted using GeoStudio SEEP/W and SLOPE/W to simulate transient rainfall infiltration and evaluate the resulting PWP and Factor of Safety (FoS) under 50-year (Case 1) and 100-year (Case 2) return-period rainfall events, applied over durations of 1, 5, 14, and 30 days. Result indicate that the slope is inherently unstable, with an initial FoS of 1.117 for both Case 1 and Case 2, confirming a consistent antecedent condition across both return-period scenarios. Prolonged 30-day rainfall caused the PWP at the ground surface to rise from an initial value of -30.3 kPa to 0 kPa in both cases, reaching full saturation by day 30 for the 50-year event (Case 1) and by Day 5 for the 100-year event (Case 2). Correspondingly, the FoS declined to 1.082 and 1.079 for Case 1 and Case 2, respectively, by the end of the simulation, remaining below the Public Works Department (PWD) of Malaysia's minimum safety requirement of 1.3 for untreated slopes throughout the simulation period. These findings highlight the importance of studying slope susceptibility to rainfall-induced instability and underscore the need for effective mitigation measures.

## 1. INTRODUCTION

Slope failure is a significant geological hazard that can lead to numerous casualties and cause extensive damage to infrastructure worldwide [1, 2]. The effects of rainfall can weaken geological materials such as minerals, rocks, soil and water [3]. Prolonged rainfall is the key factor for slope failures especially in highlands where most of the soil is soft clayey soil [4-7]. Sarawak is a tropical region with the highest rainfall ranging from 3300 mm to 4600 mm per annum, and the study area is situated in the highland of northern Sarawak. From the previous research [1, 3, 8, 9] rainfall infiltration triggers shallow and deep-seated landslide mostly in regions prone to prolonged precipitations such as Sarawak, Malaysia which is covered by 75% of residual soil average temperature and annual rainfall [10, 11]. Heavy rain induces slope instability due to increase of groundwater table [12-14] caused changes in matric suction and decreased shear strength in both unsaturated and saturated zones [15]. Porewater pressure increases when rainfall infiltrates in soil [12, 13]. The presence of groundwater can create unstable conditions that may give rise to internal soil degradation [16], typically triggered by lateral water movement, leading to a disproportionate erosion on the top layers of the soil [17]. The previous study [18] confirmed that FoS decreased from 2.44 to 1.209 due to continuous rainfall which triggers the instability of slopes. Hence, slope stability analysis plays an important role as a first step in ensuring the safety of engineering constructions like roads, embankments retaining walls etcetera [19]. Therefore, slope instability is an important concern to be considered in construction of any structure, during construction and post construction because minor slope failure can be dangerous to human lives and can lead to major damage [20, 21].

Sarawak's tropical climate is characterised by high humidity, which sustains elevated soil moisture content and considerably heightens the risk of slope instability. Historical rainfall records confirm that November through March marks the peak monsoon period in Sarawak, during which prolonged and intense rainfall substantially amplifies the likelihood of landslides and slope failures [22-24]. Intense rainfall increases both pore-water pressure and seepage force within the slope, while infiltration and subsequent retention of water increase the overall weight of the soil mass. This process reduces soil suction and, consequently, shear strength, thereby triggering slope instability [4, 25]. Furthermore, the increasing degree of saturation raises the unit weight of the soil during heavy rainfall, further elevating pore-water pressure and reducing shear strength, which in turn promotes slope movement [26]. Rainfall infiltration must therefore be considered as a coupled hydro-mechanical process to accurately predict the threshold of slope stability in tropical regions [13, 27-29]. Under natural conditions, unsaturated residual soils derive their stability

from matric suction [30-32], which effectively enhances the shear strength of the soil matrix.

While previous studies have applied GeoStudio SEEP/W and SLOPE/W to assess rainfall-induced slope instability, many of these analyses have focused on generalised rainfall conditions or a single design storm. Furthermore, site-specific investigations addressing the hydro-mechanical behaviour of slopes formed within the *Setap* Shale Formation, a lithology characterized by low permeability but a high tendency for pore-water pressure build-up under sustained infiltration, remain limited, despite this formation underlying a critical highland infrastructure corridor in northern Sarawak.Therefore, this study aims to address this gap by performing coupled transient seepage and limit-equilibrium analyses on a representative slope within the *Setap* Shale formation, directly comparing the PWP and FoS response under 50-year and 100-year return-period rainfall events. The comparative approach adopted here provides quantitative insight into how return period influences the timing and severity of stability degradation, offering practical guidance for slope design, monitoring, and mitigation planning along this and similarly susceptible infrastructure corridors.

## 2. SITE CHARACTERAZATION

### 2.1 Geographic locality and project alignment

The selected slope for this study was located at northern Sarawak at longitude 115°28'38.751"E and latitudes 4°26'11.283"N shown in Figure 1. As a critical infrastructure corridor in East Malaysia, the road project traverses the rugged, highly seasonal, topographically challenging northern highlands of Sarawak. Characterized by humid tropical climate with annual precipitation of up to 4600 mm. The combination of steep cut-slope geometries and intense, prolonged hydro-meteorological events creates a highly vulnerable environment prone to severe slope-stability failures in this area.

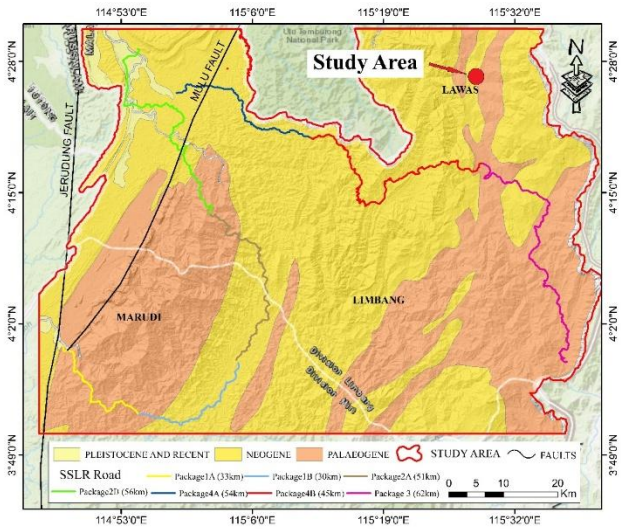



**Figure 1.** Geological maps of Sarawak and study area of selected slope

### 2.2 Geological setting and lithostratigraphy

Department of Mineral and Geoscience Malaysia (DMG) identifies the study area characterized by the *Setap* Shale Formation. According to DMG, the geological lithostratigraphic unit dates to the Oligocene and Miocene periods. The local soil formation is directly influenced by the underlying sedimentary rocks, which consist predominantly of sandstone, shale, and mudstone, with occurrences of limestone, lignite, marlstone, siltstone, and calcareous sandstone. The lithological variation reflects deposition under fluctuating marine to marginal marine environments. In terms of engineering, the geological formation of shale and mudstone is fine-grained, which makes the strength of soil decrease during saturations. The materials demonstrate low permeability yet are prone to the creation of high pore-water pressure during prolonged rainfall, increasing the possibility of rainfall-induced slope instability. The variation of permeability between shale and interbedded sandstone layers also affects the groundwater flow and seepage behavior. This makes the *Setap* Shale Formation very important for slope stability research in this work. The geological map of the study area is shown in Figure 1.

## 3. METHODOLOGY

This study investigates the mode of rainfall-induced instability at the selected slope, by considering the site's actual subsurface and climatic conditions. The flowchart of this study is shown in Figure 2. Establishing the pore-water pressure response of the slope under transient rainfall infiltration is essential prior to assessing its stability, since the mobilised shear strength along any potential sliding surface is directly governed by the effective stress state within the soil mass. To capture this behaviour. GeoStudio serves as an integrated platform for conducting coupled hydro-mechanical analyses of soil structures and is accordingly employed in this study through its SEEP/W and SLOPE/W modules.

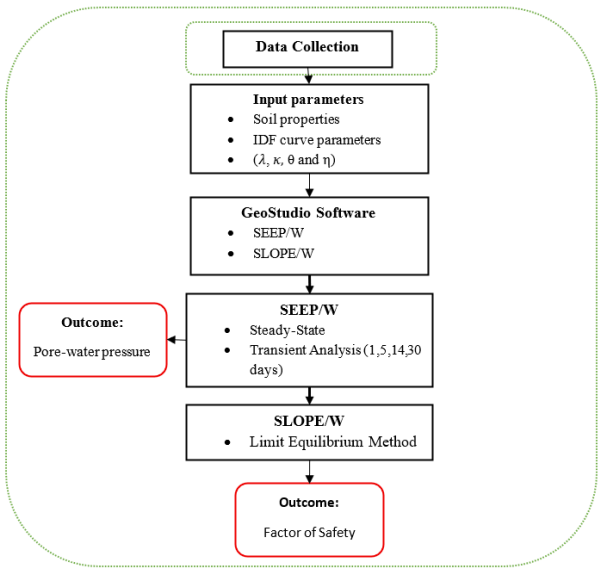



**Figure 2.** Flowchart of the study

### 3.1 Seepage analysis (SEEP/W)

SEEP/W solves the governing partial differential equation for two-dimensional transient, unsaturated–saturated seepage, based on Richards' equation:

$$\frac{\partial}{\partial x}\left(k_x \frac{\partial H}{\partial x}\right) + \frac{\partial}{\partial y}\left(k_y \frac{\partial H}{\partial y}\right) + Q = \frac{\partial \theta_w}{\partial t} \quad (1)$$

where, $k_x$ and $k_y$ are the hydraulic conductivities in the $x$- and $y$-directions, respectively (a function of matric suction for unsaturated soil), $H$ is the total hydraulic head, $Q$ is the applied boundary flux, $\theta_w$ is the volumetric water content, and $t$ is time.

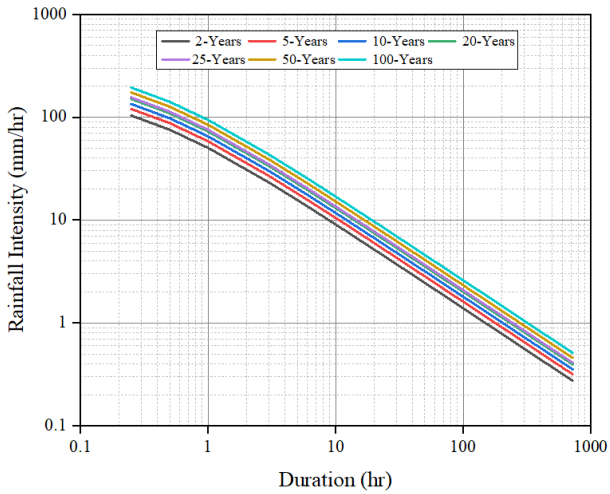



**Figure 3.** IDF curve for the selected grid coordinate

The rainfall intensities applied as boundary conditions in the transient analysis were derived from the Intensity-Duration-Frequency (IDF) curve shown in Figure 3. Four independent transient analyses, corresponding to durations of 1,5, 14 and 30 days were performed in this study, each initiated from the same steady-state initial condition and applying its own duration-averaged rainfall intensity as a constant flux boundary condition for that analysis full duration only. The average rainfall intensity is determined by Eq. (2):

$$i = \frac{\lambda T^K}{(d+\theta)^n} \quad (2)$$

where, $i$ is the rainfall intensity, $t$ is the duration, and $T$ is the return period in years. The parameter $\lambda$ represents the regional location parameter, an empirical constant that reflects the local rainfall characteristics of the study area. The exponent $\kappa$ is related to the return period and governs how rainfall intensity increases with increasing return period, while $\theta$ is the duration correction factor, an empirical constant that adjusts the duration term to improve the fit of the intensity-duration relationship and $\eta$ is the exponent related to rainfall duration, controlling the rate at which rainfall intensity decreases as the storm duration increases. All four parameters ($\lambda$, $\kappa$, $\theta$, and $\eta$) shown in Table 1 are empirical constants specific to the study location, derived from the isopleth maps provided by the Department of Irrigation and Drainage (DID) Malaysia.

Two cases were established, Case 1 refers to the water flux boundary condition (Table 2) applied with 50-year return period, while Case 2 for a 100-year return period.

The hydraulic conductivity and volumetric water content functions required to solve this equation for each soil layer are defined by the Soil-Water Characteristic Curve (SWCC), as described in Section 3.1.1. A steady-state analysis was first performed to establish the initial pore-water pressure distribution within the slope prior to rainfall, which then served as the initial condition for each of the four independent transient analyses.

**Table 1.** Empirical values based on selected grid

| Grid No. | λ | κ | θ | η |
|---|---|---|---|---|
| 395 | 55.212 | 0.1599 | 0.2805 | 0.8228 |

**Table 2.** Boundary flux rates across rainfall events

| Case | 1 | 2 |
|---|---|---|
| Day | Intensity (m/sec) | |
| 1 | 2.05E-06 | 2.32E-06 |
| 5 | 5.28E-07 | 6.22E-07 |
| 14 | 2.22E-07 | 2.67E-07 |
| 30 | 1.17E-07 | 1.43E-07 |

3.1.1 Subsurface conditions and estimated hydraulic properties

The subsurface profile of this study was characterized through borehole investigations. The stratigraphy at the study area shows a complex layering of cohesive soils overlying weathered rock. As illustrated in the slope cross-section Figure 4 the stratigraphy is dominated by silty CLAY and weathered MUDSTONE.

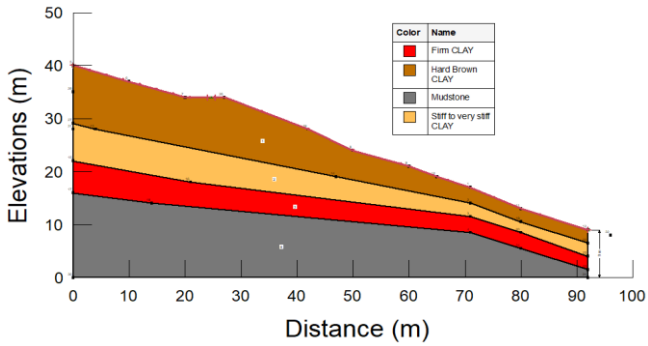
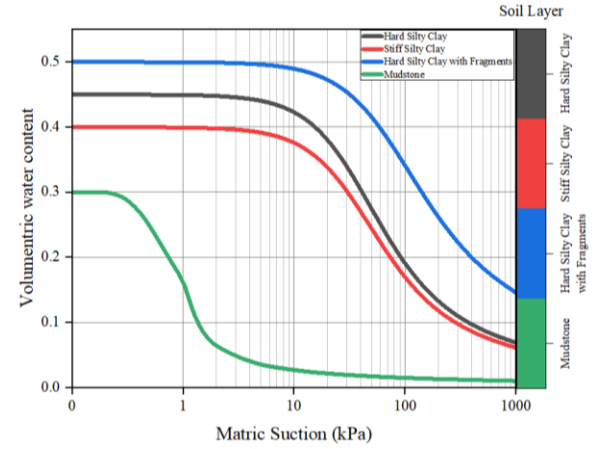


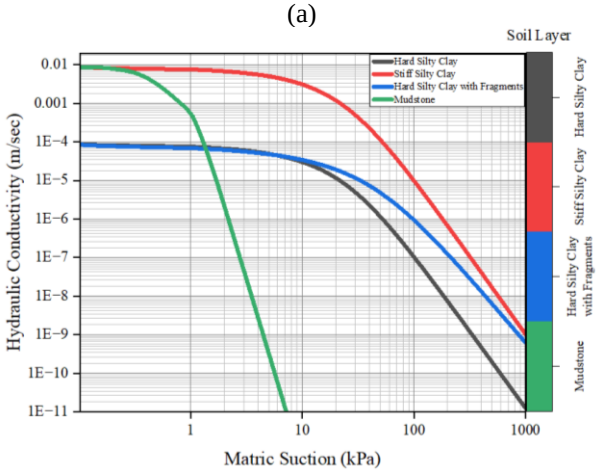

**Figure 4.** Slope cross-section showing subsurface stratigraphy

**Table 3.** Soil type and parameters used in SEEP/W and SLOPE/W

| | SEEP/W | | | | SLOPE/W | |
|---|---|---|---|---|---|---|
| **Soil Type** | **ksat (m/s)** | **θsa** | **θres** | **Phi** | **C (kpa)** | **Unit weight kN/m³** |
| Hard Brown CLAY | $1\times10^{-9}$ | 0.45 | 0.05 | 28 | 5 | 19 |
| Firm CLAY | $1\times10^{-7}$ | 0.4 | 0.05 | 24 | 2 | 16 |
| Stiff to very stiff CLAY | $1\times10^{-9}$ | 0.5 | 0.05 | 28 | 3 | 17 |
| | **Generalized Hoek-Brown criteria** | | | | | |
| **Stone Type** | **Unit weight** | **UCS intact** | **mi** | **GSI** | **D** | **ksat (m/s)** | **θsa** | **θres** |
| MUDSTONE | 25 | 20000kpa | 19 | 35 | 1 | $1\times10^{-7}$ | 0.3 | 0.03 |




(a)




(b)

**Figure 5.** (a) SWCC of soil layer and (b) hydraulic conductivity function

The profile consists of the following layers shown in Table 3. The Soil-Water Characteristic Curve (SWCC) and hydraulic conductivity were estimated for all layers of soil for unsaturated soil behaviour representation. The values of saturated water content and residual water content were derived from published empirical data, and both plots were created using the sampling function in SEEP/W software. Different soil layers have different water retention characteristics Figure 5(a), which are due to different soil properties. Similarly, the corresponding variations of hydraulic conductivity with increasing matric suction are presented in Figure 5(b).

The hydraulic properties were estimated using the standard material functions of the SEEP/W software based on the assigned soil types and the available soil parameters. These estimated functions were then used in the seepage model to define the hydraulic behaviour of the soil layers during the analysis. The SWCC and hydraulic conductivity functions obtained were then used to define the hydraulic properties required for the transient seepage analysis. Since the hydraulic functions were estimated from standard material functions and not directly obtained from laboratory testing, these are considered as estimated parameters and used to provide the required input conditions for the numerical analysis of both Cases 1 and 2.

### 3.2 Stability analysis (SLOPE/W)

SLOPE/W employs the limit equilibrium method (LEM), where the potential sliding mass is discretised into vertical slices. Force and moment equilibrium are assessed for each slice to determine the FoS, defined as the ratio of available shear strength to mobilised shear stress (Eq. (3)). The Morgenstern–Price method was adopted in this study, as it satisfies both force and moment equilibrium for every slice using a side-force function, making it suitable for slopes with irregular geometry and heterogeneous, layered soil profiles. The pore-water pressure field generated by each four independent SEEP/W transient analyses (durations of 1, 5, 14, and 30) was directly linked to the corresponding SLOPE/W stability analysis, allowing the temporal evolution of FoS to be evaluated as a direct function of the rainfall-induced pore-water pressure response. To ensure a consistent basis for comparison between the two return periods, both Case 1 (50-year) and Case 2 (100-year) were modelled using an identical finite-element mesh (10 m global element size) and identical slope geometry, with pore-water pressure and stability results extracted at fixed, identical coordinates (ground surface, mid-depth, and deep base along a common vertical section) for both cases.

Numerical simulation of slope stability was conducted by using the parameters of soil type in Table 3. For SLOPE/W the soil layer was characterized by effective friction angle ranging from 24° to 28° and cohesions (c) values between 2 kPa and 5 kPa. The generalised Hoek-Brown failure criterion was applied to mudstone layer due to highly fractured, Grade III/IV mass structure [33]. These parameters are essential for conducting LEM slope stability analyses. The Mohr–Coulomb failure criterion was selected for the soil layers due to its effectiveness in modelling the cohesive and frictional behaviour of tropical residual soils. The SEEP/W utilised saturated permeability values and volumetric water content to simulate rainfall infiltration.

The soil profile and geotechnical parameters adopted in this study were established from a site investigation programme conducted for the proposed SSLR 1, comprising a series of Standard Penetration Test (SPT) boreholes. Soil samples retrieved during the SPT boring operations were subjected to laboratory testing to determine the strength and index properties of each soil layer, including the effective friction angle, cohesion, and unit weight. The resulting geotechnical dataset, together with the corresponding borehole-derived slope geometry, was provided by the engineering consultant responsible for the site investigation and forms the empirical basis for the material properties applied in the numerical model. This approach ensures that the strength parameters employed in the SLOPE/W analysis are representative of the actual subsurface conditions along the SSLR 1 alignment, rather than assumed or generalized values.

Factor of Safety (FoS) of LEM theory is defined as ratio of maximum shear strength ($\tau_f$) to the mobilized shear stress ($\tau_m$):

$$\text{FoS} = \frac{\tau_f}{\tau_m} = \frac{c' + (\sigma - u)\tan\phi'}{\tau_m} \quad (3)$$

where, $\tau$ is the shear strength, $c'$ is the effective cohesion, $\sigma$ is the total normal stress, $u_w$ is the pore-water pressure, and $\phi'$ is the effective angle of internal friction. The term $(\sigma - u_w)$ represents the effective normal stress acting on the potential failure surface, which decreases as pore-water pressure increases during rainfall infiltration, thereby reducing the available shear strength and consequently the FoS of the slope.

The Morgenstern-Price Method was applied to force and moment equilibrium providing the detail analysis of the slip surface during the FoS determinations. In Malaysia, the minimum FoS requirement for slope is 1.3 for untreated slope meanwhile the minimum global shall be 1.5 for treated slope [34]. Table 4 shows Slope stability classifications.

**Table 4.** Factor of Safety (FoS) classification

| FoS | Classification Based on PWD Malaysia |
|---|---|
| FoS ≥ 1.5 | Treated Slope is Stable |
| FoS ≥ 1.3 | Untreated Slope is Stable |
| FoS < 1.3 | Unstable (Need to be treated) |

Note: PWD = Public Works Department.

## 4. RESULT AND DISCUSSION

This section presents the analysis of pore-water pressure distributions and the effects of water infiltration on the slope stability of the selected slope.

### 4.1 Initial and transient pore-water pressure

The analysis was performed to study the changes in pore-water pressure and matric suction at various locations downslope under the given rainfall conditions. The variation of pore-water pressure with time for Case 1 and Case 2 is shown in Figure 6.

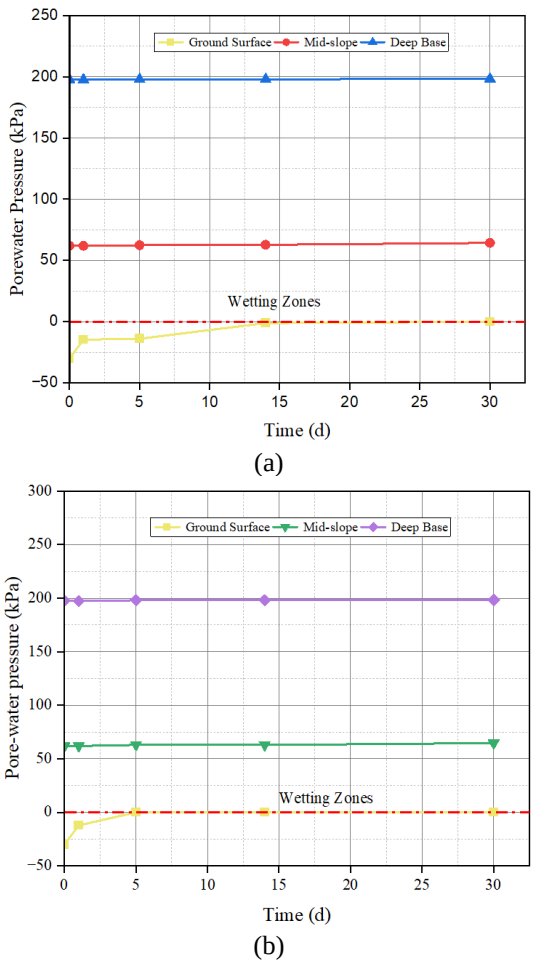



**Figure 6.** Pore-water pressure distribution in time (a) Case 1 and (b) Case 2

Negative pore-water pressure was observed in the unsaturated zone under the initial conditions (day 0), which implies the presence of matric suction. As rainfall infiltrated the slope, the pore-water pressure gradually rose, and the magnitude of negative pore-water pressure decreased. This indicates a progressive decrease in matric suction with increasing wetness of the soil.

Both Case 1 and Case 2 share an identical initial (steady-state) pore-water pressure distribution prior to the onset of rainfall, confirming a consistent antecedent condition across both return-period scenarios: the ground surface pore-water pressure was −30.03 kPa in both cases, corresponding to an initial critical FoS of 1.117 in each case. Following the onset of rainfall, the two cases diverge according to their respective return-period intensities. For Case 1 (50-year), the ground surface pore-water pressure rose from −30.03 kPa to −14.56 kPa by Day 1, −13.91 kPa by Day 5, and −1.31 kPa by Day 14, reaching 0 kPa (full saturation) only by Day 30. For Case 2 (100-year), the ground surface pore-water pressure rose more rapidly, from −30.03 kPa to −12.20 kPa by Day 1, reaching 0 kPa by Day 5 and remaining at full saturation through Day 14 and Day 30. This confirms that the higher-intensity 100-year event drives the slope to full surface saturation considerably faster than the 50-year event, despite both starting from the same initial condition.

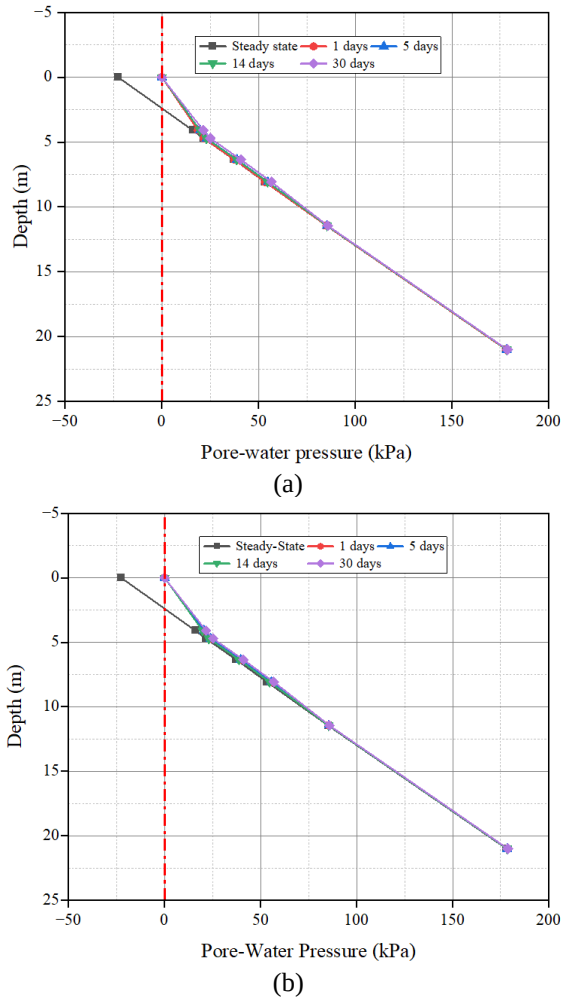



**Figure 7.** Porewater pressure distribution in depth (a) Case 1 and (b) Case 2

Pore-water pressure increases and the corresponding decrease of matric suction can diminish the contribution of

suction to the shear strength of unsaturated soil [35]. Therefore, long-term rainfall can decrease the stability of a slope, especially when the pore-water pressure, particularly as the soil approaches or reaches saturation.

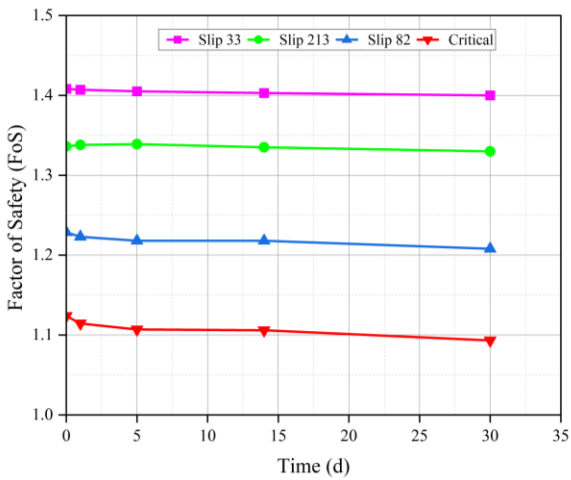
The pore-water pressure distributions along soil depth over 30 days of transient rainfall infiltration for Case 1 and Case 2 are shown in Figure 7. For Case 1 (Figure 7(a)), the initial steady-state profile shows a matric suction of approximately 22.5 kPa at the ground surface, with the initial groundwater table (0 kPa pore-water pressure) located at a depth of approximately 2.4 m. Upon the onset of rainfall, the surface pore-water pressure rises rapidly, reaching full saturation (0 kPa) as early as Day 1, after which the near-surface zone within the upper 6 m wetting zone remains close to saturation for the remainder of the 30-day simulation.

Both Case 1 and Case 2 share an identical Day 0 steady-state profile (Figure 7(a) and 7(b)), confirming the standardized antecedent condition between the two cases. As with Case 1, the surface pore-water pressure in Case 2 also reaches full saturation (0 kPa) as early as Day 1 of rainfall. The two profiles are not, however, identical once rainfall begins: at corresponding depths within the upper 6 m wetting zone, Case 2 exhibits marginally higher pore-water pressures than Case 1 from Day 1 onward (for example, approximately 20.4 kPa versus 18.6 kPa at 4.08 m depth on Day 1), consistent with its higher first-day rainfall intensity, although this difference is small relative to the overall steady-state-to-saturated transition and is not readily distinguishable at the scale of Figure 7. Below approximately 6 m depth, pore-water pressure increases linearly with depth and remains largely unaffected by surface infiltration in either case.

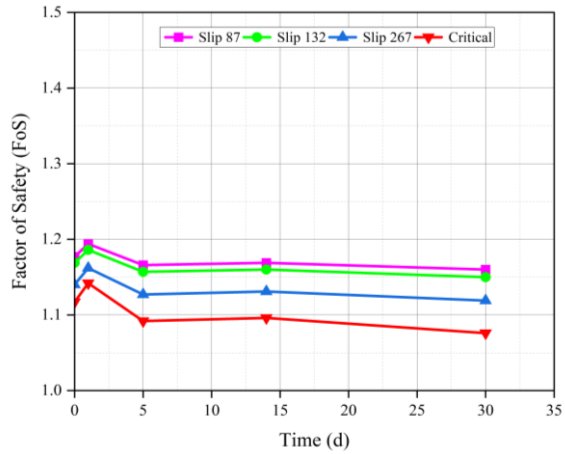
### 4.2 Factor of Safety

Figure 8(a) and Figure 8(b) illustrates the FoS against time. The FoS decrease with the increase of rainfall durations.

Figures 9–11 show the inverse relationship between rainfall duration and the FoS of the slope. As shown in Figure 8, both the 50-year (Case 1) and 100-year (Case 2) rainfall events produced a general decline in critical FoS as rainfall duration increased, consistent with the rise in pore-water pressure and the corresponding reduction in effective stress and shear strength discussed in Section 4.1. The most pronounced reduction in both cases occurred within the first five days of rainfall, after which the rate of decline became more gradual as the soil profile approached full saturation.

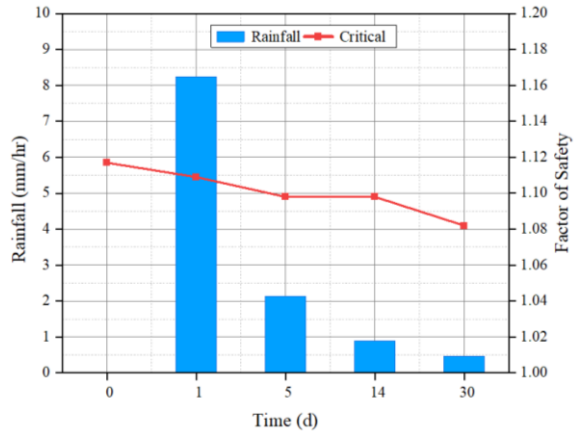



(a)

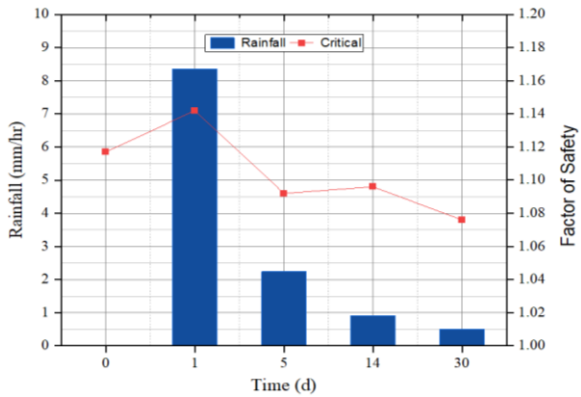



(b)

**Figure 8.** Factor of Safety (FoS) versus rainfall durations for (a) Case 1 and (b) Case 2

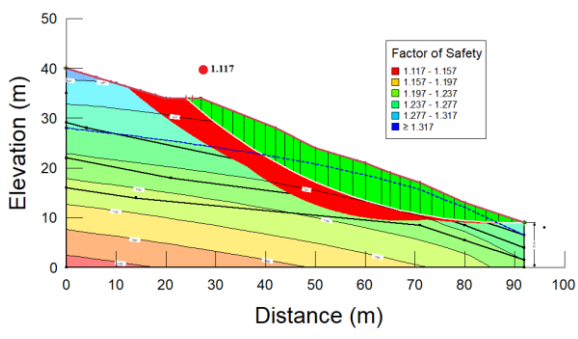



(a)

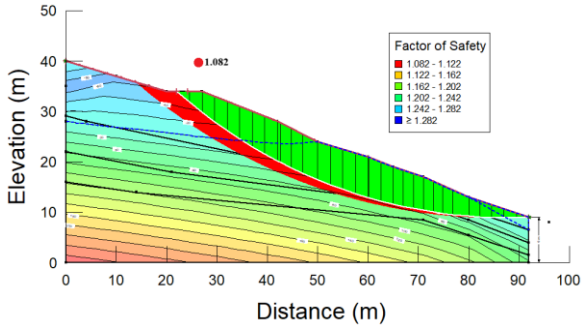



(b)

**Figure 9.** Rainfall intensity and critical Factor of Safety (FoS) versus time for (a) Case 1 and (b) Case 2

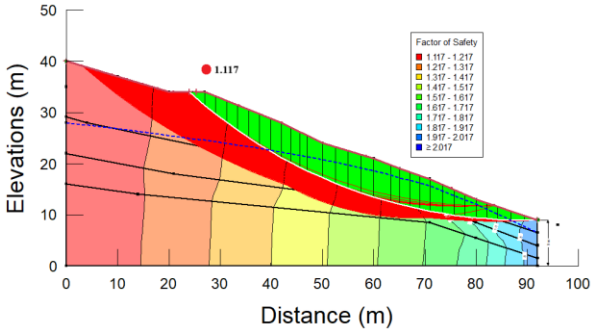



(a)

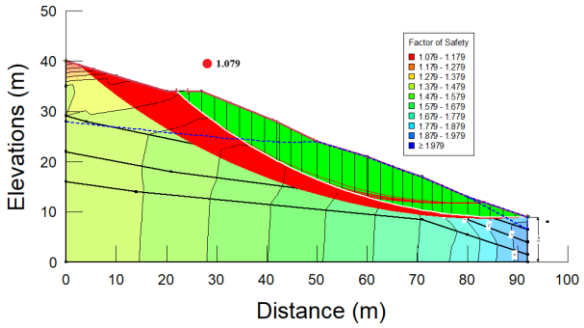



(b)

**Figure 10.** Factor of Safety (FoS) versus rainfall durations of transient of case 1 (a) Initial FoS at Day 0 and (b) Final FoS at Day 30




(a)




(b)

**Figure 11.** Factor of Safety (FoS) versus rainfall durations of transient of case 2 (a) Initial FoS at Day 0 and (b) Final FoS at Day 30

Both Case 1 and Case 2 began from an identical initial critical FoS of 1.117, confirming the consistency of the standardized antecedent condition. For Case 1, the critical FoS declined from 1.117 on Day 0 to 1.109 on Day 1, 1.098 on Day 5, 1.098 on Day 14, and 1.082 on Day 30, as shown in Figure 10. For Case 2, the critical FoS declined from the same initial value of 1.117, rose briefly to 1.142 on Day 1 (reflecting the short-term influence of the high first-day rainfall intensity before pore-water pressure effects fully propagate to the critical slip surface), then declined to 1.092 on Day 5, 1.096 on Day 14, and 1.079 on Day 30, as shown in Figure 11. Despite Case 2 experiencing higher rainfall during the first day, Case 1 ultimately underwent the greater overall reduction in stability, suggesting that the 50-year event's slip surface geometry and wetting-front progression made it more sensitive to sustained infiltration than the 100-year event.

From the safety compliance perspective, the result is critical. During the 30 days of simulations, the factor of safety consistently remains above the 1.0 FoS following standard, beginning at an identical initial value of 1.117 for both cases and concluding at 1.082 for Case 1 and 1.079 for Case 2. Moreover, the result does not comply with the JKR standard with a minimum criterion of 1.3 and 1.5, as shown by the red dashes in the graph. The difference between the measured FoS and the regulatory standard indicates that the study area is particularly exposed to rainfall-induced instability and the necessity to apply effective mitigation strategies to guarantee long-term stability.

## 5. CONCLUSIONS

This study investigated the effect of rainfall infiltration on slope stability. The analysis for seepage and slope stability is implemented by using GeoStudio software. The result of the analysis shows several critical insights were identified observing the geotechnical behavior of the selected slope during prolonged precipitation events:

(1) The results show that water infiltrated into the soil leads to a rapid increase in ground-surface pore-water pressure (PWP) from an identical initial value of -30.03 kPa to zero kPa, with the time to reach full saturation depending on the return period: by Day 30 for Case 1 and by Day 5 for Case 2. This rise shows the loss of matric suction of soil, and the soil becomes fully saturated, which can cause slope failure to occur.

(2) An inverse relationship was observed between the duration of rainfall and FoS. The initial values FoS are 1.117 for both cases, already dropped below the 1.3 threshold, indicating that the slope did not meet the minimum safety requirement for untreated slopes even prior to the onset of rainfall. After 30 days of precipitation, the FoS further reduced to 1.082 and 1.079 for the 50-year and 100-year events, respectively.

(3) It is essential to state that, at no stage during the simulation did the investigated slope meet the JKR minimum safety requirement of 1.3 for untreated slopes.

In conclusion, the high rainfall intensity and the geological characteristics of the *Setap* Shale Formation make the northern Sarawak highlands highly susceptible to rainfall-induced landslides. These results stress the importance of effective mitigation and stabilisation strategies, such as improved drainage systems or structural reinforcements, to ensure the long-term stability and safety of this critical situation.

## ACKNOWLEDGMENT

The authors wish to acknowledge the Universiti Malaysia Sarawak (UNIMAS) for supporting this work under the grant number UNI/F02/GRADUATES/85657/2023.

## REFERENCES

[1] Jia, J., Mao, C., Tenorio, V.O. (2024). Slope stability considering multi-fissure seepage under rainfall conditions. Scientific Reports, 14(1): 11662. https://doi.org/10.1038/s41598-024-62387-3

[2] Liu, Y., Gao, C., Zhuang, W., et al. (2025). Prediction and early warning analysis of reservoir bank slopes based on anti-sliding stability evolution. Geoscience Frontiers, 16(5): 102113.

https://doi.org/10.1016/j.gsf.2025.102113
[3] Liu, F., Dong, Z., Khayatnezhad, M. (2026). Parametric assessment of rainfall-related slope stability through SRM modeling and orthogonal experimental design: Insights from the Zhuquedong slope, China. Scientific Reports, 16(1): 13091. https://doi.org/10.1038/s41598-026-43289-y
[4] Rosly, M.H., Mohamad, H.M., Bolong, N., Harith, N.S.H. (2023). Relationship of rainfall intensity with slope stability. Civil Engineering Journal, 9: 75-82. https://doi.org/10.28991/CEJ-SP2023-09-06
[5] Li, X., Li, X., Yang, Z., Zhang, S., Shen, P. (2026). Physics-informed neural networks for efficient probabilistic analysis of regional rainfall-induced landslides. Geoscience Frontiers, 17(6): 102388. https://doi.org/10.1016/j.gsf.2026.102388
[6] Lei, X., Zhang, W., He, S., et al. (2025). Numerical modelling of rainfall-induced internal erosion process within vegetated deposited slopes. Journal of Rock Mechanics and Geotechnical Engineering, 17(8): 5170-5187. https://doi.org/10.1016/j.jrmge.2025.02.013
[7] Huang, G., Ma, Q., Wu, Y. (2025). Rainfall infiltration of multi-layer soil slope with a modified Green-Ampt model. KSCE Journal of Civil Engineering, 29(5): 100131. https://doi.org/10.1016/j.kscej.2024.100131
[8] Wang, M., Wang, C. (2026). Slope reliability analysis of tailings dam under coincidence of rainfall and pseudo-static motions. Scientific Reports. https://doi.org/10.1038/s41598-026-68328-6
[9] Showkat, M., Ghani, S., Paramasivam, P., Yusuf, M. (2026). Automated slope stability assessment using modified Morgenstern-Price method and machine learning integration. Scientific Reports, 16(1): 9952. https://doi.org/10.1038/s41598-026-38670-w
[10] Idrus, J., Hamzah, N., Ramli, R., Nujid, M.M., Sadikon, S.F. (2023). Enhancing slope stability with different slope stabilization measures: A case study using SLOPE/W software. Jurnal Kejuruteraan, 35(6): 1427-1434. https://doi.org/10.17576/jkukm-2023-35(6)-15
[11] Ullah, R., Abdullah, R.A., Kassim, A., Yunus, N.Z.M., Sendo, H. (2021). Assessment of residual soil properties for slope stability analysis. International Journal of GEOMATE, 21(86): 72-80. https://doi.org/10.21660/2021.86.j2282
[12] Dhanai, P., Singh, V.P., Soni, P. (2022). Rainfall triggered slope instability analysis with changing climate. Indian Geotechnical Journal, 52(2): 477-492. https://doi.org/10.1007/s40098-021-00581-0
[13] Sajwan, A., Mhaski, S., Ramana, G.V. (2025). Modelling rainfall-induced seepage, internal erosion, and slope instability via a deterministic multi-phase SPH framework. Computational Particle Mechanics, 12(6): 5481-5505. https://doi.org/10.1007/s40571-025-01088-8
[14] Zhong, Z., Hu, B., Li, J., Sheng, J., Wan, C. (2025). Impact of rainfall dry-wet cycles on slope deformation and landslide prediction in open-pit mines: A case study of Mohuandang Landslide, Emeishan, China. Results in Engineering, 26: 105011. https://doi.org/10.1016/j.rineng.2025.105011
[15] Wang, Z., Li, X., Yin, S., Du, X. (2022). Analysis of rainfall infiltration and improvement of the analytical solution of safety factors on unsaturated inner dump slopes: A case study. Processes, 10(11): 2407. https://doi.org/10.3390/pr10112407
[16] Lei, X., Zhang, W., Chen, X., Ming, L. (2023). Influence of internal erosion on rainfall-induced instability of layered deposited-soil slopes. Mathematics, 11(20): 4348. https://doi.org/10.3390/math11204348
[17] Zheng, Y., Hu, W., van Asch, T., Li, Y., Fan, Y. (2024). Experimental study on the failure mechanisms of non-cohesive soil landslide dams with different scales. Engineering Geology, 333: 107489. https://doi.org/10.1016/j.enggeo.2024.107489
[18] Fadilah, S., Luknanto, D. (2020). Effects of heavy rainfall on the slope stability – A case study on Imogiri Cemetery: The graveyard complex of Mataram Royal Kings. E3S Web of Conferences, 200: 02006. https://doi.org/10.1051/e3sconf/202020002006
[19] Liu, F. (2020). Stability analysis of geotechnical slope based on strength reduction method. Geotechnical and Geological Engineering, 38(4): 3653-3665. https://doi.org/10.1007/s10706-020-01243-3
[20] Ramesh, C.P., Girish, B.S. (2022). Analysis of climate changes and slope instability factors triggered by natural rainfall. International Journal of Scientific Research and Engineering Trends, 8(1): 374-378.
[21] Ullah, S., Khan, M.U., Rehman, G. (2020). A brief review of the slope stability analysis methods. Geological Behavior, 4(2): 73-77. https://doi.org/10.26480/gbr.02.2020.73.77
[22] Chin, J.B., Takaijudin, H.B., Shafiai, S.H.B. (2022). Assessing downstream flood risk under changing climate for Bakun Dam in Sarawak. International Journal of Environmental Impacts, 5(4): 316-330. https://doi.org/10.2495/EI-V5-N4-316-330
[23] Lias, R., Jais, I.B.M., Lat, D.C. (2022). Climatic influence on slope failure: A case study at Kem Terendak, Melaka. International Journal of Sustainable Construction Engineering and Technology, 13(1): 39-49. https://doi.org/10.30880/ijscet.2022.13.01.004
[24] Rosly, M.H., Mohamad, H.M., Bolong, N., Harith, N.S.H. (2022). An overview: Relationship of geological condition and rainfall with landslide events at East Malaysia. Trends in Sciences, 19(8): 3464. https://doi.org/10.48048/tis.2022.3464
[25] Savi, S., Comiti, F., Strecker, M.R. (2021). Pronounced increase in slope instability linked to global warming: A case study from the eastern European Alps. Earth Surface Processes and Landforms, 46(7): 1328-1347. https://doi.org/10.1002/esp.5100
[26] Muntohar, A.S., Azhar, M., Jotisankasa, A., Chaiprakaikeow, S., Chung, C.C. (2022). Evaluation the slope movement and effectiveness the remedial measures of volcanic residual soil in Yogyakarta, Indonesia. Research Square (Preprint). https://www.researchsquare.com/article/rs-2266790/v1
[27] Ma, X., Tao, Y., Lu, M., Sharma, A., Zhang, J. (2025). Reliability analysis of soil slopes stabilized with piles under rainfall. Journal of Rock Mechanics and Geotechnical Engineering, 17(11): 6951-6963. https://doi.org/10.1016/j.jrmge.2024.12.015
[28] Zhang, J., Yu, H., Liu, Y., Han, Z. (2026). Real-time slope stability analysis of gentle expansive soil slope under rainfall infiltration condition. Soils and Foundations, 66(3): 101788. https://doi.org/10.1016/j.sandf.2026.101788
[29] Xu, J., Fang, K. (2026). Deformation characteristics of unsaturated slope during post-rainfall earthquake:

Insights from centrifuge and numerical modeling. Journal of Rock Mechanics and Geotechnical Engineering, 18(1): 380-397. https://doi.org/10.1016/j.jrmge.2025.03.004
[30] Peranic, J., Jagodnik, V., Arbanas, Z. (2019). Rainfall infiltration and stability analysis of an unsaturated slope in residual soil from flysch rock mass. In 17th European Conference on Soil Mechanics and Geotechnical Engineering, Reykjavík, IS, pp. 1-8. https://doi.org/10.32075/17ECSMGE-2019-0906
[31] Najar, I.A., Ahmadi, R., Khalik, Y.K.A., Taib, S.N.L., Sutan, N.B.M., Ramli, N.H.B. (2023). Soil suffusion under the dual threat of rainfall and seismic vibration. International Journal of Design & Nature and Ecodynamics, 18(4): 849-860. https://doi.org/10.18280/ijdne.180411
[32] Rahimi, A., Rahardjo, H., Leong, E.C. (2011). Effect of antecedent rainfall patterns on rainfall-induced slope failure. Journal of Geotechnical and Geoenvironmental Engineering, 137(5): 483-491. https://doi.org/10.1061/(asce)gt.1943-5606.0000451
[33] Shen, J., Priest, S.D., Karakus, M. (2012). Determination of Mohr-Coulomb shear strength parameters from generalized Hoek-Brown criterion for slope stability analysis. Rock Mechanics and Rock Engineering, 45(1): 123-129. https://doi.org/10.1007/s00603-011-0184-z
[34] Jabatan Kerja Raya. (2010). Guidelines for slope design (JKR 21500-0011-10). Slope Engineering Branch, Public Works Department Malaysia. https://exam.jkr.gov.my/document/get/88.
[35] Hakro, M.R., Almani, Z., Channa, M.A., Jokhio, J. (2024). Numerical modelling of matric suction in unsaturated soil under shallow foundation under varying soil and hydrological conditions. Jurnal Kejuruteraan, 36(2): 569-580. https://doi.org/10.17576/jkukm-2024-36(2)-17

## NOMENCLATURE

| | |
|---|---|
| $i$ | Rainfall intensity, m/s |
| $d$ | Storm duration, days |
| $T$ | Average recurrence interval (return period), years |
| $K$ | Fitting exponent related to return period (IDF equation) |
| $n$ | Fitting exponent related to storm duration (IDF equation) |
| $c'$ | Effective cohesion, kPa |
| $c$ | Cohesion (Mohr–Coulomb), kPa |
| $u$ | Pore-water pressure, kPa |
| $D$ | Disturbance factor (Hoek–Brown criterion) |
| $mi$ | Intact rock material constant (Hoek–Brown criterion) |
| $ksat$ | Saturated hydraulic conductivity. m/s |

### Greek symbols

| | |
|---|---|
| $\lambda$ | Regional location parameter (IDF equation) |
| $\theta$ | Duration correction constant (IDF equation) |
| $\varphi'$ | Effective angle of internal friction, $^{o}$ |
| $\varphi$ | Friction angle (Mohr–Coulomb), $^{o}$ |
| $\sigma$ | Total normal stress, kpa |
| $\tau f$ | Maximum (available) shear strength, kpa |
| $\tau m$ | Mobilized shear stress |
| $\theta sa$ | Saturated volumetric water content |
| $\theta res$ | Residual volumetric water content |

### Abbreviations

| | |
|---|---|
| PWP | Pore-Water Pressure |
| FOS | Factor of Safety |
| SEEP/W | Seepage analysis module (GeoStudio) |
| SLOPE/W | Slope stability analysis module (GeoStudio) |
| LEM | Limit Equilibrium Method |
| IDF | Intensity–Duration–Frequency |
| SWCC | Soil-Water Characteristic Curve |
| PWD | Public Works Department (Malaysia) |
| JKR | Jabatan Kerja Raya (Malaysian Public Works Department) |
| DMG | Department of Minerals and Geosciences (Malaysia) |
| S.I. | Site Investigation |
| GSI | Geological Strength Index |
| UCS | Unconfined Compressive Strength |
| 2D | Two-Dimensional |
| UNIMAS | Universiti Malaysia Sarawak |